

First model-independent determination of the relative strong phase between D^0 and $\bar{D}^0 \rightarrow K_S^0 \pi^+ \pi^-$ and its impact on the CKM Angle γ/ϕ_3 measurement

R. A. Briere,¹ H. Vogel,¹ P. U. E. Onyisi,² J. L. Rosner,² J. P. Alexander,³ D. G. Cassel,³ J. E. Duboscq,^{3,*} R. Ehrlich,³ L. Fields,³ L. Gibbons,³ R. Gray,³ S. W. Gray,³ D. L. Hartill,³ B. K. Heltsley,³ D. Hertz,³ J. M. Hunt,³ J. Kandaswamy,³ D. L. Kreinick,³ V. E. Kuznetsov,³ J. Ledoux,³ H. Mahlke-Krüger,³ D. Mohapatra,³ J. R. Patterson,³ D. Peterson,³ D. Riley,³ A. Ryd,³ A. J. Sadoff,³ X. Shi,³ S. Stroiney,³ W. M. Sun,³ T. Wilksen,³ S. B. Athar,⁴ J. Yelton,⁴ P. Rubin,⁵ S. Mehrabyan,⁶ N. Lowrey,⁶ M. Selen,⁶ E. J. White,⁶ J. Wiss,⁶ R. E. Mitchell,⁷ M. R. Shepherd,⁷ D. Besson,⁸ T. K. Pedlar,⁹ D. Cronin-Hennessy,¹⁰ K. Y. Gao,¹⁰ J. Hietala,¹⁰ Y. Kubota,¹⁰ T. Klein,¹⁰ R. Poling,¹⁰ A. W. Scott,¹⁰ P. Zweber,¹⁰ S. Dobbs,¹¹ Z. Metreveli,¹¹ K. K. Seth,¹¹ B. J. Y. Tan,¹¹ A. Tomaradze,¹¹ J. Libby,¹² L. Martin,¹² A. Powell,¹² G. Wilkinson,¹² H. Mendez,¹³ J. Y. Ge,¹⁴ D. H. Miller,¹⁴ V. Pavlunin,¹⁴ B. Sanghi,¹⁴ I. P. J. Shipsey,¹⁴ B. Xin,¹⁴ G. S. Adams,¹⁵ D. Hu,¹⁵ B. Moziak,¹⁵ J. Napolitano,¹⁵ K. M. Ecklund,¹⁶ Q. He,¹⁷ J. Insler,¹⁷ H. Muramatsu,¹⁷ C. S. Park,¹⁷ E. H. Thorndike,¹⁷ F. Yang,¹⁷ M. Artuso,¹⁸ S. Blusk,¹⁸ N. Horwitz,¹⁸ S. Khalil,¹⁸ J. Li,¹⁸ R. Mountain,¹⁸ K. Randrianarivony,¹⁸ N. Sultana,¹⁸ T. Skwarnicki,¹⁸ S. Stone,¹⁸ J. C. Wang,¹⁸ L. M. Zhang,¹⁸ G. Bonvicini,¹⁹ D. Cinabro,¹⁹ M. Dubrovin,¹⁹ A. Lincoln,¹⁹ P. Naik,²⁰ J. Rademacker,²⁰ D. M. Asner,²¹ K. W. Edwards,²¹ J. Reed,²¹ A. N. Robichaud,²¹ and G. Tatishvili²¹

(CLEO Collaboration)

¹*Carnegie Mellon University, Pittsburgh, Pennsylvania 15213, USA*

²*Enrico Fermi Institute, University of Chicago, Chicago, Illinois 60637, USA*

³*Cornell University, Ithaca, New York 14853, USA*

⁴*University of Florida, Gainesville, Florida 32611, USA*

⁵*George Mason University, Fairfax, Virginia 22030, USA*

⁶*University of Illinois, Urbana-Champaign, Illinois 61801, USA*

⁷*Indiana University, Bloomington, Indiana 47405, USA*

⁸*University of Kansas, Lawrence, Kansas 66045, USA*

⁹*Luther College, Decorah, Iowa 52101, USA*

¹⁰*University of Minnesota, Minneapolis, Minnesota 55455, USA*

¹¹*Northwestern University, Evanston, Illinois 60208, USA*

¹²*University of Oxford, Oxford OX1 3RH, UK*

¹³*University of Puerto Rico, Mayaguez, Puerto Rico 00681*

¹⁴*Purdue University, West Lafayette, Indiana 47907, USA*

¹⁵*Rensselaer Polytechnic Institute, Troy, New York 12180, USA*

¹⁶*Rice University; Houston; TX 77005, USA*

¹⁷*University of Rochester, Rochester, New York 14627, USA*

¹⁸*Syracuse University, Syracuse, New York 13244, USA*

¹⁹*Wayne State University, Detroit, Michigan 48202, USA*

²⁰*University of Bristol, Bristol BS8 1TL, UK*

²¹*Carleton University, Ottawa, Ontario, Canada K1S 5B6*

(Dated: March 9, 2009)

Abstract

We exploit the quantum coherence between pair-produced D^0 and \bar{D}^0 in $\psi(3770)$ decays to make a first determination of the relative strong phase differences between $D^0 \rightarrow K_S^0 \pi^+ \pi^-$ and $\bar{D}^0 \rightarrow K_S^0 \pi^+ \pi^-$, which are of great importance in determining the CKM angle γ/ϕ_3 in $B^- \rightarrow D^0(\bar{D}^0)K^-$ decays. Using 818 pb^{-1} of e^+e^- collision data collected with the CLEO-c detector at $E_{\text{cm}} = 3.77$ GeV, we employ a binned Dalitz-plot analysis of $K_S^0 \pi^+ \pi^-$ and $K_L^0 \pi^+ \pi^-$ decays recoiling against flavor-tagged, CP-tagged and $K_S^0 \pi^+ \pi^-$ tagged events to determine these strong phase differences.

*Deceased

I. INTRODUCTION

A central goal of flavor physics is the determination of all elements of the CKM matrix [1], magnitudes and phases. Of the three angles of the $b - d$ CKM triangle, denoted α , β , and γ by some, ϕ_2 , ϕ_1 , and ϕ_3 by others, the least-well determined is γ/ϕ_3 , the phase of V_{ub} relative to V_{cb} . It is of great interest to determine γ/ϕ_3 using the decay $B^\pm \rightarrow K^\pm \tilde{D}^0$, since in this mode, the γ/ϕ_3 value obtained is expected to be insensitive to new physics effects in B decays. Here, \tilde{D}^0 is either D^0 or \bar{D}^0 , and both decay to the same final state, and so their amplitudes add. Sensitivity to the angle γ/ϕ_3 comes from the interference between two Cabibbo-suppressed diagrams: $b \rightarrow c\bar{u}s$, giving rise to $B^- \rightarrow K^- D^0$, and the color and CKM suppressed process $b \rightarrow u\bar{c}s$, giving rise to $B^- \rightarrow K^- \bar{D}^0$. One of the most promising \tilde{D}^0 decays for measuring γ/ϕ_3 using this method is $\tilde{D}^0 \rightarrow K_S^0 \pi^+ \pi^-$, because it is Cabibbo favored (CF) for both D^0 and \bar{D}^0 decays, thus providing large event yields. To make use of this decay, however, the interference effects between $B^- \rightarrow K^- \bar{D}^0 (\rightarrow K_S^0 \pi^+ \pi^-)$ and $B^- \rightarrow K^- D^0 (\rightarrow K_S^0 \pi^+ \pi^-)$ need to be understood. These interference effects can be understood and measured using CLEO-c data.

We first write the amplitude for the B^\pm decay as follows:

$$\mathcal{A}(B^\pm \rightarrow K^\pm \tilde{D}^0, \tilde{D}^0 \rightarrow K_S^0 \pi^+ \pi^-(x, y)) \propto f_D(x, y) + r_B e^{i\theta_\pm} f_{\bar{D}}(x, y). \quad (1)$$

Here, $x \equiv m_{K_S^0 \pi^+}^2$, $y \equiv m_{K_S^0 \pi^-}^2$ are the Dalitz-plot variables in the \tilde{D}^0 decay, $f_D(x, y)(f_{\bar{D}}(x, y))$ is the amplitude for $D^0(\bar{D}^0)$ decay to $K_S^0 \pi^+ \pi^-$ at (x, y) , r_B is the ratio of the suppressed to favored amplitudes, and $\theta_\pm \equiv \delta_B \pm \gamma$, where δ_B is the strong phase shift between the color-favored and color-suppressed amplitudes. Ignoring the second-order effects of charm mixing and CP violation [2, 3], we have $f_{\bar{D}}(x, y) = f_D(y, x)$, and Eq. 1 can then be rewritten as:

$$\mathcal{A}(B^\pm \rightarrow K^\pm \tilde{D}^0, \tilde{D}^0 \rightarrow K_S^0 \pi^+ \pi^-(x, y)) \propto f_D(x, y) + r_B e^{i\theta_\pm} f_D(y, x). \quad (2)$$

The square of the amplitude clearly depends on the phase difference $\Delta\delta_D \equiv \delta_D(x, y) - \delta_D(y, x)$, where $\delta_D(x, y)$ is the phase of $f_D(x, y)$. Thus, for the determination of γ/ϕ_3 , one must know $\Delta\delta_D(x, y)$.

Previous analyses extracted $\Delta\delta_D(x, y)$ by fitting a flavor-tagged $D^0 \rightarrow K_S^0 \pi^+ \pi^-$ Dalitz plot to a model for D^0 decay involving various 2-body intermediate states [4, 5, 6]. Such an approach introduces a $7^\circ \sim 9^\circ$ model uncertainty in the value of γ/ϕ_3 ,¹ which would be a limiting uncertainty for LHCb [7] and future B -factory experiments.

In the analysis presented here, we employ a model-independent approach to obtain $\Delta\delta_D(x, y)$ as suggested by Giri *et al.* [2], by exploiting the quantum coherence of $D^0 - \bar{D}^0$ pairs at the $\psi(3770)$. Because of this quantum correlation, $K_S^0 \pi^+ \pi^-$ and $K_L^0 \pi^+ \pi^-$ decays recoiling against flavor tags, CP-tags, and $D^0 \rightarrow K_S^0 \pi^+ \pi^-$ tags, taken together provide direct sensitivity to the quantities $\cos \Delta\delta_D$ and $\sin \Delta\delta_D$. This measurement will result in a substantial reduction in the systematic uncertainty associated with the interference effects between $B^- \rightarrow K^- \bar{D}^0 (\rightarrow K_S^0 \pi^+ \pi^-)$ and $B^- \rightarrow K^- D^0 (\rightarrow K_S^0 \pi^+ \pi^-)$.

¹ BaBar claims 5° uncertainty on γ/ϕ_3 in [5] by combining $K_S^0 K^+ K^-$ and $K_S^0 \pi^+ \pi^-$ modes.

II. FORMALISM

Giri *et al.* proposed [2] a model-independent procedure for obtaining $\Delta\delta_D(x, y)$, as follows. The Dalitz plot is divided into $2\mathcal{N}$ bins, symmetrically about the line $x = y$. The bins are indexed from $-i$ to i , excluding zero. The coordinate exchange $x \leftrightarrow y$ thus corresponds to the exchange of bins $i \leftrightarrow -i$. The number of events in the i -th bin of a flavor-tagged $K_S^0\pi^+\pi^-$ Dalitz plot from a D^0 decay is then expressed as:

$$K_i = A_D \int_i |f_D(x, y)|^2 dx dy = A_D F_i, \quad (3)$$

where A_D is a normalization factor. The interference between the D^0 and \bar{D}^0 amplitudes is parameterized by two quantities

$$c_i \equiv \frac{1}{\sqrt{F_i F_{-i}}} \int_i |f_D(x, y)| |f_D(y, x)| \cos[\Delta\delta_D(x, y)] dx dy, \quad (4)$$

and

$$s_i \equiv \frac{1}{\sqrt{F_i F_{-i}}} \int_i |f_D(x, y)| |f_D(y, x)| \sin[\Delta\delta_D(x, y)] dx dy, \quad (5)$$

where the integral is performed over a single bin. The parameters c_i and s_i are the amplitude-weighted averages of $\cos \Delta\delta_D$ and $\sin \Delta\delta_D$ over each Dalitz-plot bin. It is important to note that c_i and s_i depend only on the D^0 decay, not the B decay, and therefore these quantities can be measured using CLEO-c data. In principle they could be left as free parameters in a $\tilde{D}^0 \rightarrow K_S^0\pi^+\pi^-$ Dalitz-plot analysis from B^\pm decays, but their values can be more precisely determined from correlated $D^0\bar{D}^0$ pairs produced in CLEO-c.

Though the original idea of Giri *et al.* was to divide the Dalitz plot into square bins [2], Bondar *et al.* noted [8] that increased sensitivity is obtained if the bins are chosen to minimize the variation in $\Delta\delta_D$ over each bin. Thus, we divide the Dalitz phase space into \mathcal{N} bins of equal size with respect to $\Delta\delta_D$ as predicted by the BaBar isobar model [4]. In the half of the Dalitz plot $m^2(K_S^0\pi^+) < m^2(K_S^0\pi^-)$, the i^{th} bin is defined by the condition

$$2\pi(i - 3/2)/\mathcal{N} < \Delta\delta_D(x, y) < 2\pi(i - 1/2)/\mathcal{N}, \quad (6)$$

The $-i^{\text{th}}$ bin is defined symmetrically in the lower portion of the Dalitz plot. Such a binning with $\mathcal{N} = 8$ is shown in Fig. 1. One might suspect that because we are using a model to determine our bins, we are not free of model dependence. In fact *any* binning is correct in that it will give a correct, unbiased answer for γ/ϕ_3 , at the cost of larger uncertainties compared to an optimal binning with respect to $\Delta\delta_D$.

We now describe how CLEO-c data can be used to determine c_i and s_i . The event yields in the i^{th} bin of both flavor-tagged and CP-tagged $\tilde{D}^0 \rightarrow K_S^0\pi^+\pi^-$ Dalitz plot are required. Because the $\psi(3770)$ has $C = -1$, the CP of the $\tilde{D}^0 \rightarrow K_S^0\pi^+\pi^-$ decay can be determined by reconstructing the companion \tilde{D}^0 in a CP eigenstate. With a CP-tagged $\tilde{D}^0 \rightarrow K_S^0\pi^+\pi^-$ decay, the amplitude is given by:

$$f_{CP\pm}(x, y) = \frac{1}{\sqrt{2}} [f_D(x, y) \pm f_D(y, x)], \quad (7)$$

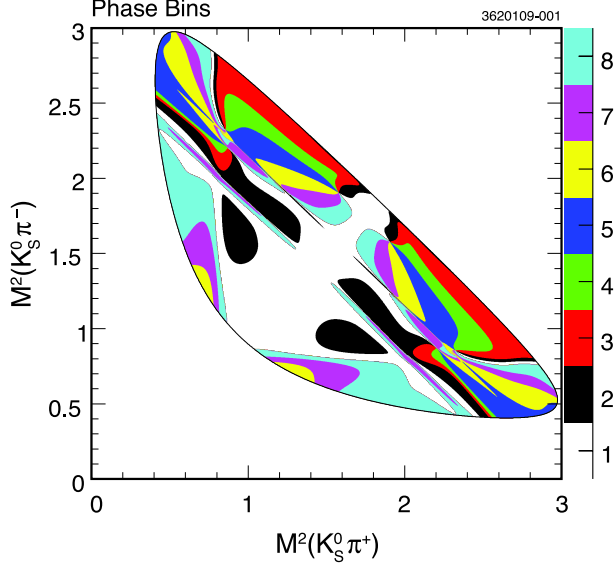


FIG. 1: Phase binning of the $D^0 \rightarrow \bar{K}_S^0 \pi^+ \pi^-$ Dalitz plot.

for CP-even and CP-odd states of a $\tilde{D}^0 \rightarrow K_S^0 \pi^+ \pi^-$ decay. Since the event rate is proportional to the square of this amplitude, the number of events in the i^{th} bin of a CP-tagged Dalitz plot is then:

$$M_i^\pm = h_{CP\pm} (K_i \pm 2c_i \sqrt{K_i K_{-i}} + K_{-i}), \quad (8)$$

where $h_{CP\pm} = S^\pm / 2S_f$ is a normalization factor that depends on the number, S_f , of single flavor-tagged signal decays, and the number, S^\pm , of single CP-tagged signal decays. Thus, access to c_i is enabled by measuring the number of events, M_i^\pm , in a CP-tagged $K_S^0 \pi^+ \pi^-$ Dalitz plot, and the number of events, K_i , in a flavor-tagged $K_S^0 \pi^+ \pi^-$ Dalitz plot.

Unfortunately, as evident from Eq. 4, the sign of $\Delta\delta_D$ is undetermined in each of the i bins. However, sensitivity to both c_i and s_i can be obtained by analyzing $D^0 \rightarrow K_S^0 \pi^+ \pi^-$ vs. $\bar{D}^0 \rightarrow K_S^0 \pi^+ \pi^-$ data. The amplitude for $\psi(3770)$ decays to two $K_S^0 \pi^+ \pi^-$ decays is as follows:

$$f(x, y, x', y') = \frac{f_D(x, y) f_D(y', x') - f_D(x', y') f_D(y, x)}{\sqrt{2}}. \quad (9)$$

The primed and unprimed Dalitz-plot coordinates correspond to the Dalitz-plot variables of the two $\tilde{D}^0 \rightarrow K_S^0 \pi^+ \pi^-$ decays. Defining M_{ij} as the event rate in the i^{th} bin of the first and the j^{th} bin of the second $\tilde{D}^0 \rightarrow K_S^0 \pi^+ \pi^-$ Dalitz plots, respectively, we have:

$$M_{ij} = h_{corr} (K_i K_{-j} + K_{-i} K_j - 2\sqrt{K_i K_{-j} K_{-i} K_j} (c_i c_j + s_i s_j)). \quad (10)$$

Here, $h_{corr} = N_{D\bar{D}} / 2S_f^2$, where $N_{D\bar{D}}$ is the number of $D\bar{D}$ pairs, and as before S_f is the number of flavor-tagged signal decays. Equation 10 then relates the product $(c_i c_j + s_i s_j)$ to the measured yields of events in the flavor-tagged $\tilde{D}^0 \rightarrow K_S^0 \pi^+ \pi^-$ Dalitz plot ($K_{i,j}$'s) and the yields in the $D^0 \rightarrow K_S^0 \pi^+ \pi^-$ vs. $\bar{D}^0 \rightarrow K_S^0 \pi^+ \pi^-$ (M_{ij} 's) Dalitz plots. The sensitivity to this product leads to a four-fold ambiguity: change of sign of all c_i or all s_i . In combination with

the CP-tagged analysis though, where the sign of c_i is determined, this reduces to a two-fold ambiguity. One of the two solutions can be chosen based on a weak model assumption [4].

The decay $D^0 \rightarrow K_L^0 \pi^+ \pi^-$, due to its close relationship with $D^0 \rightarrow K_S^0 \pi^+ \pi^-$, can be used to further improve the c_i and s_i determination. Since the K_S^0 and K_L^0 mesons are of opposite CP, and we assume the convention that $A(D^0 \rightarrow K_S^0 \pi^+ \pi^-) = A(\bar{D}^0 \rightarrow K_S^0 \pi^- \pi^+)$, it then follows that $A(D^0 \rightarrow K_L^0 \pi^+ \pi^-) = -A(\bar{D}^0 \rightarrow K_L^0 \pi^- \pi^+)$. Then, for $K_L^0 \pi^+ \pi^-$, the Dalitz-plot rates of Eq. 8 (CP vs. $D^0 \rightarrow K_S^0 \pi^+ \pi^-$) and Eq. 10 ($D^0 \rightarrow K_S^0 \pi^+ \pi^-$ vs. $\bar{D}^0 \rightarrow K_S^0 \pi^+ \pi^-$) become:

$$M_i^\pm = h_{CP\pm}(K'_i \mp 2c'_i \sqrt{K'_i K'_{-i}} + K'_{-i}), \quad (11)$$

$$M_{ij} = h_{corr}[K_i K'_{-j} + K_{-i} K'_j + 2\sqrt{K_i K'_{-j} K_{-i} K'_j}(c_i c'_j + s_i s'_j)], \quad (12)$$

for CP vs. $D^0 \rightarrow K_L^0 \pi^+ \pi^-$ and $D^0 \rightarrow K_S^0 \pi^+ \pi^-$ vs. $\bar{D}^0 \rightarrow K_L^0 \pi^+ \pi^-$, respectively, where c'_i , s'_i are associated with $D^0 \rightarrow K_L^0 \pi^+ \pi^-$ decay.

For $D^0 \rightarrow K_L^0 \pi^+ \pi^-$ decays to benefit our determination of c_i and s_i , we must determine the differences $\Delta c_i \equiv c'_i - c_i$, and $\Delta s_i \equiv s'_i - s_i$. In addition to the relative sign change in Eq. 11 and Eq. 12, doubly Cabibbo suppressed decays (DCSD) of D^0/\bar{D}^0 also contribute with opposite signs in $D^0 \rightarrow K_S^0 \pi^+ \pi^-$ and $D^0 \rightarrow K_L^0 \pi^+ \pi^-$ decays. We can see this by inspecting the D^0 decay amplitude for each Dalitz plot

$$A(K_S^0 \pi^+ \pi^-) = \frac{1}{\sqrt{2}}[A(K^0 \pi^+ \pi^-) + A(\bar{K}^0 \pi^+ \pi^-)], \quad (13)$$

$$A(K_L^0 \pi^+ \pi^-) = \frac{1}{\sqrt{2}}[A(K^0 \pi^+ \pi^-) - A(\bar{K}^0 \pi^+ \pi^-)]. \quad (14)$$

The effect of this relative minus sign is to introduce a 180° phase difference for all DCSD K^* resonances in the $K_L^0 \pi^+ \pi^-$ model. We can use U-spin symmetry to relate the amplitudes for resonances of definite CP eigenvalue, e.g. $K_{S,L}^0 \rho^0(770)$. We find that these states acquire a factor of $r e^{i\delta}$. To convert a $D^0 \rightarrow K_S^0 \pi^+ \pi^-$ model to the corresponding $D^0 \rightarrow K_L^0 \pi^+ \pi^-$ model, we multiply all DCSD amplitudes by -1 and multiply each CP eigenstate amplitude by $(1 - 2r e^{i\delta})$, with $r = \tan^2 \theta_C$ and $\delta = 0^\circ$ fixed for every resonance (here θ_C is the Cabibbo angle). We then determine central values for the corrections, $\Delta c_i \equiv c'_i - c_i$, $\Delta s_i \equiv s'_i - s_i$ using the $D^0 \rightarrow K_S^0 \pi^+ \pi^-$ BaBar model [4]. We ascribe uncertainty to both the choice of r and δ , as well as the usage of the BaBar model to determine the uncertainties on Δc_i and Δs_i . The former are estimated by varying the phase δ between 0 and 2π , and r by $\pm 50\%$. For the latter, we estimate Δc_i and Δs_i using the Belle [6] and CLEO [9] $D^0 \rightarrow K_S^0 \pi^+ \pi^-$ isobar model fits, and take the largest resulting deviation from the value found with the BaBar model as a model-dependent systematic uncertainty. The total systematic uncertainties in the corrections are the quadrature sum of these two uncertainties. The central values and uncertainties on Δc_i and Δs_i are shown in Table I.

III. EVENT SELECTION

We analyze 818 pb $^{-1}$ of e^+e^- collision data produced by the Cornell Electron Storage Ring (CESR) at $E_{\text{cm}} = 3.77$ GeV and collected with the CLEO-c detector. The CLEO-c detector

TABLE I: Predicted values for Δc_i and Δs_i with the systematic uncertainties.

i	Δc_i	Δs_i
0	0.099 ± 0.040	-0.034 ± 0.068
1	0.167 ± 0.029	-0.064 ± 0.084
2	0.327 ± 0.122	-0.013 ± 0.097
3	0.253 ± 0.192	0.133 ± 0.136
4	0.077 ± 0.061	0.041 ± 0.080
5	0.220 ± 0.084	-0.038 ± 0.065
6	0.416 ± 0.160	0.095 ± 0.063
7	0.184 ± 0.024	0.015 ± 0.086

is a general purpose solenoidal detector which includes a tracking system for measuring momentum and specific ionization (dE/dx) of charged particles, a Ring Imaging Cherenkov detector (RICH) to aid in particle identification, and a CsI calorimeter for detection of electromagnetic showers. The CLEO-c detector is described in detail elsewhere [10].

Standard CLEO-c selection criteria for π^\pm , K^\pm , π^0 , and K_S^0 candidates are used, and are described in Ref. [11]. To distinguish electrons from hadrons, we use a multivariate discriminant [12] that combines information from the ratio of the energy deposited in the calorimeter to the measured track momentum (E/p), ionization energy loss in the tracking chamber (dE/dx), and the ring-imaging Cherenkov counter (RICH). For K_S^0 decays, we select candidates with $|M(\pi^+\pi^-) - M_{K_S^0}| < 7.5 \text{ MeV}/c^2$, and require the decay vertex to be separated from the interaction region with a significance greater than two standard deviations (except for $D^0 \rightarrow K_S^0\pi^+\pi^-$ vs. $\bar{D}^0 \rightarrow K_S^0\pi^+\pi^-$ candidates). Reconstruction of $\eta \rightarrow \gamma\gamma$ proceeds analogously to $\pi^0 \rightarrow \gamma\gamma$, with the requirement that $|M(\gamma\gamma) - M_\eta| < 42 \text{ MeV}/c^2$. We form $\omega \rightarrow \pi^+\pi^-\pi^0$ candidates and require their mass to be within 20 MeV of the nominal ω mass [13].

In this analysis, we reconstruct D^0 mesons in several flavor-tagged modes, CP-tagged modes, and in $K_S^0\pi^+\pi^-$. From these selected events, we also reconstruct the companion D^0 from the $\psi(3770)$ decay in either $K_S^0\pi^+\pi^-$ or $K_L^0\pi^+\pi^-$ to form “double-tags”. The single tags yields enter our analysis through the S_f and S^\pm factors, whereas the double-tags provide the K_i , M_i and M_{ij} yields across their respective Dalitz plots. The double-tagged events we consider are shown in Table II (all the notations include charge conjugate if not otherwise specified.). We thus consider flavor tags: $K^-\pi^+$, $K^-\pi^+\pi^0$, $K^-\pi^+\pi^+\pi^-$; semileptonic tag: $K^-e^+\nu$; CP-even tags: K^+K^- , $\pi^+\pi^-$, $K_S^0\pi^0\pi^0$, $K_L^0\pi^0$; and CP-odd tags: $K_S^0\pi^0$, $K_S^0\eta$, $K_S^0\omega$, with $\pi^0/\eta \rightarrow \gamma\gamma$, $\omega \rightarrow \pi^+\pi^-\pi^0$, and $K_S^0 \rightarrow \pi^+\pi^-$. We also reconstruct double-tag (DT) events with $\tilde{D}^0 \rightarrow K_{S,L}^0\pi^+\pi^-$ vs $\tilde{D}^0 \rightarrow K_S^0\pi^+\pi^-$ as discussed in the preceding section. We do not reconstruct $K_L^0\pi^+\pi^-$ in some DT modes when there are two missing particles ($K^-e^+\nu$, and $K_L^0\pi^0$ cases) or the backgrounds are large (as for $K_S^0\pi^0\pi^0$, and $K_S^0\omega$).

The event yield in the i^{th} Dalitz-plot bin of each tagged $\tilde{D}^0 \rightarrow K_{S,L}^0\pi^+\pi^-$ sample is determined by evaluating the phase difference for each data point according to the BaBar isobar model. The contribution of each isobar to the total amplitude is evaluated as a function of all three invariant mass-squared combinations computed directly from the four-momentum of the \tilde{D} daughters as described in Ref. [14]. The phase difference is well defined beyond and continues smoothly across the kinematically allowed Dalitz-plot boundary as shown in Fig. 2. A small number of candidate events ($\sim 1\text{-}3\%$ depending on tag and signal

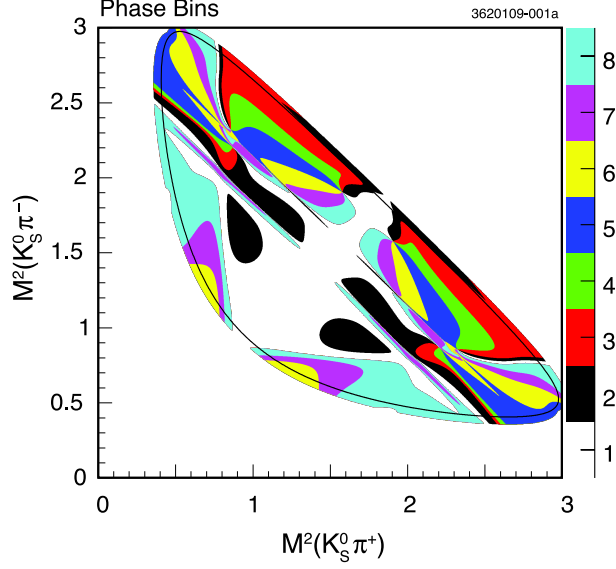


FIG. 2: Binning of the $D^0 \rightarrow \bar{K}_S^0 \pi^+ \pi^-$ Dalitz plot with respect to $\Delta\delta_D$. The bins are extended beyond the kinematically allowed Dalitz-plot boundary.

mode) included in this analysis are reconstructed outside the kinematically allowed region due to finite detector resolution.

TABLE II: Reconstructed Double Tag modes.

Mode	$K_S^0 \pi^+ \pi^-$	$K_L^0 \pi^+ \pi^-$
Flavor Tags		
$K^- \pi^+$	×	×
$K^- \pi^+ \pi^0$	×	×
$K^- \pi^+ \pi^+ \pi^-$	×	×
$K^- e^+ \nu$	×	
CP-Even Tags		
$K^+ K^-$	×	×
$\pi^+ \pi^-$	×	×
$K_S^0 \pi^0 \pi^0$	×	
$K_L^0 \pi^0$	×	
CP-Odd Tags		
$K_S^0 \pi^0$	×	×
$K_S^0 \eta$	×	×
$K_S^0 \omega$	×	
$K_S^0 \pi^+ \pi^-$	×	×

A. Single Tags

The $\psi(3770)$ resonance is below threshold for $D\bar{D}\pi$ production, and so the events of interest, $e^+e^- \rightarrow \psi(3770) \rightarrow D\bar{D}$, have D mesons with energy equal to the beam energy and a unique momentum. Thus, for identifying D^0 candidates, we follow Mark III [15] and define two kinematic variables: the beam-constrained candidate mass, $M_{BC} \equiv \sqrt{E_0^2/c^4 - \mathbf{P}_D^2/c^2}$, where \mathbf{P}_D is the D^0 candidate momentum and E_0 is the beam energy, and $\Delta E \equiv E_D - E_0$, where E_D is the sum of the D^0 candidate daughter energies. Candidate tags are required to have ΔE within about 3 standard deviations of zero [16].

For events with a $K^-\pi^+$, K^+K^- , and $\pi^+\pi^-$ single-tag (ST) that have no additional charged particles, we apply additional selection requirements to suppress cosmic ray muons and Bhabha events. We do not allow tracks identified as electrons or muons to be used in the tag. We demand evidence of the other D by requiring at least one electromagnetic shower in the calorimeter above 50 MeV not associated with the tracks of the tag, where a single minimum ionizing particle deposits the equivalent of 200 MeV. For K^+K^- ST candidates, additional geometric requirements are needed to remove doubly radiative Bhabha events followed by pair conversion of a radiated photon. We accept only one candidate per mode per event; when multiple candidates are present, we choose the one with smallest $|\Delta E|$.

The resulting M_{BC} distributions are shown in Fig. 3. Each distribution is fit to a signal shape derived from simulated signal events and to a background ARGUS [17] threshold function. The ST yield is given by the area in the signal peak in the mass region from $1.86 < M_{BC} < 1.87$ GeV.

B. Double tags with $K_S^0\pi^+\pi^-$

We form $K_S^0\pi^+\pi^-$ DTs by combining a $K_S^0\pi^+\pi^-$ tag with a ST candidate. We choose one DT candidate per mode per event with \bar{M} closest to the measured D^0 mass, where $\bar{M} \equiv [M(D^0) + M(\bar{D}^0)]/2$.

Since the $D^0 \rightarrow K_S^0\pi^+\pi^-$ vs. $\bar{D}^0 \rightarrow K_S^0\pi^+\pi^-$ sample plays a key role in extracting s_i values, we drop the requirement on the flight distance significance for K_S^0 candidates to increase the statistics. We find 421 $D^0 \rightarrow K_S^0\pi^+\pi^-$ vs. $\bar{D}^0 \rightarrow K_S^0\pi^+\pi^-$ candidates which include about 9% background. We increase the yield by about 15% (additional 54 candidates, $\sim 15\%$ background) by reconstructing the $K_S^0\pi^+\pi^-$ vs. $K_S^0\pi^+\pi^-$ candidates when one π^\pm is not reconstructed. The presence of the π^\pm is inferred from the missing four-momentum calculated from the well known initial state and the reconstructed particles.

C. Double tags with $K^-e^+\nu$

Candidate $K^-e^+\nu$ vs. $K_S^0\pi^+\pi^-$ DTs are reconstructed by combining a $K_S^0\pi^+\pi^-$ ST candidate with a kaon candidate and an electron candidate from the remainder of the event. Events with more than two additional tracks (aside from the $K_S^0\pi^+\pi^-$ daughters) are vetoed. Signal discrimination for $D \rightarrow K^-e^+\nu$ uses the variable $U \equiv E_{miss} - c|\vec{\mathbf{p}}_{miss}|$, where E_{miss} and $\vec{\mathbf{p}}_{miss}$ are the missing energy and momentum in the semileptonic D^0 meson decay, calculated using the difference of the four-momenta of the tag and that of the K^- and e^+ candidates. For correctly identified events, $U = 0$, since only the neutrino is undetected. After all selection criteria are applied, multiple candidates are rare for $K^-e^+\nu$. The U

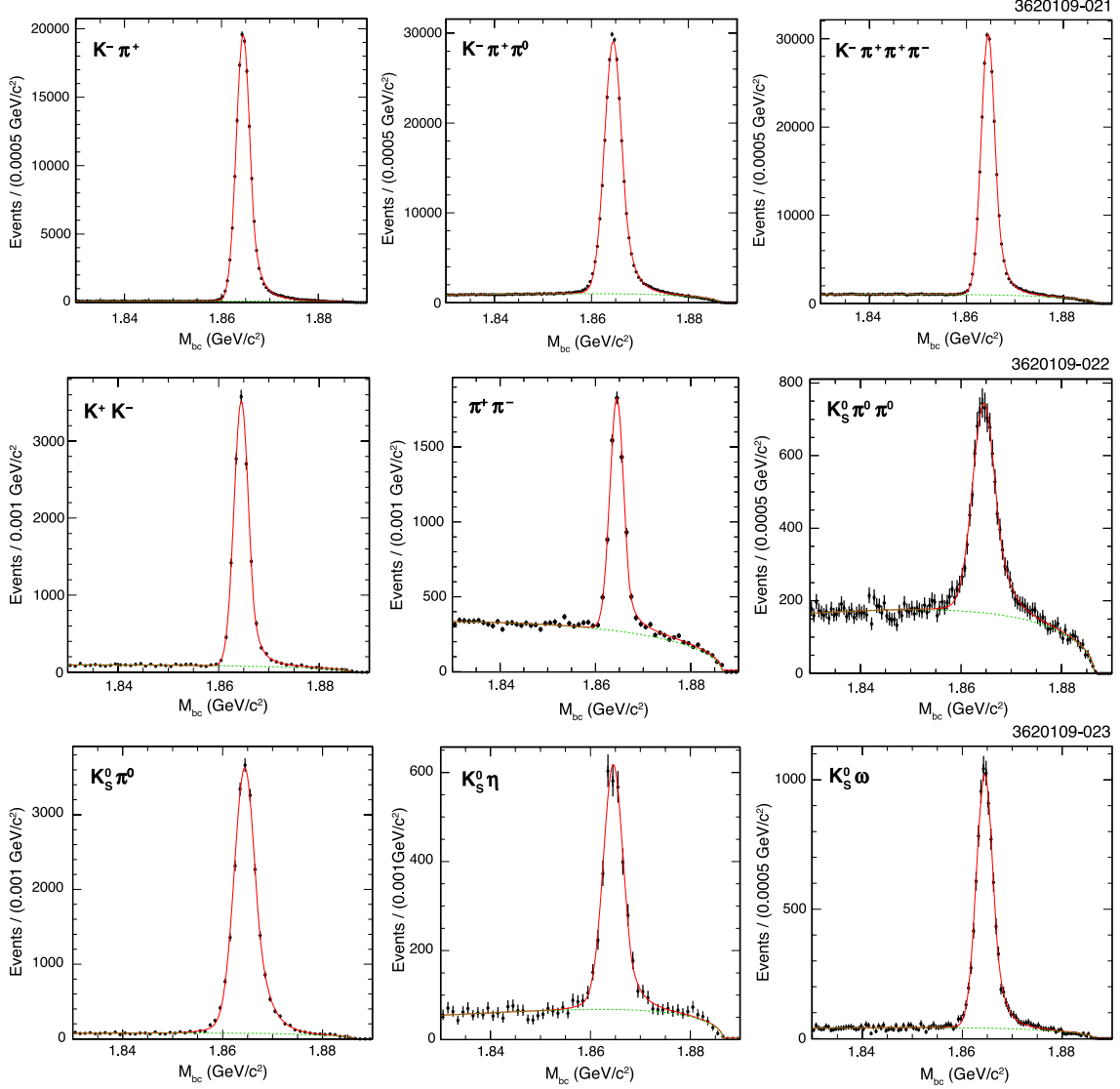


FIG. 3: Data M_{bc} distribution for various tag modes. The solid lines show the total fits, and the dashed lines show the background shapes.

distribution for $D^0 \rightarrow K^- e^+ \nu$ candidates is shown in Fig. 4. The points with error bars are data and the shaded histogram represents a simulation of the background, which is less than 1% in the signal region, $|U| < 50$ MeV.

D. Double tags with $K_L^0 \pi^0$

The $K_S^0 \pi^+ \pi^-$ vs. $K_L^0 \pi^0$ DT mode is reconstructed with a missing mass technique since the K_L^0 mesons produced at CLEO-c are not reconstructed. A fully reconstructed $K_S^0 \pi^+ \pi^-$ ST is combined with a π^0 candidate, and we compute the recoil-mass squared against the ST- π^0 system, M_{miss}^2 . Signal $K_L^0 \pi^0$ decays are identified by a peak in M_{miss}^2 at $M_{K_L^0}^2$. Backgrounds from $D \rightarrow K_S^0 \pi^0$, $\pi^0 \pi^0$, and $\eta \pi^0$ are suppressed by vetoing events with additional unassigned charged particles, or $\eta \rightarrow \gamma \gamma$ or $\pi^0 \rightarrow \gamma \gamma$ candidates. We further suppress backgrounds by

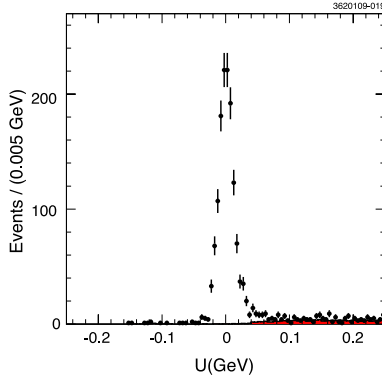


FIG. 4: $U \equiv E_{miss} - c|\vec{\mathbf{p}}_{miss}|$ distribution for $K^- e^+ \nu$ in events with a $D^0 \rightarrow K_S^0 \pi^+ \pi^-$ signal candidate. The points are data and the shaded histogram represents a simulation of the backgrounds.

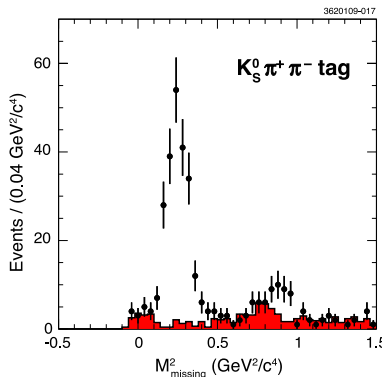


FIG. 5: M_{miss}^2 distributions for $K_L^0 \pi^0$ when one D is identified as $K_S^0 \pi^+ \pi^-$. Shaded histogram represents simulation of the backgrounds. The enhancement of data relative to simulation $\sim 0.9 \text{ GeV}^2/c^4$ corresponds to the decay $K^{*0} \pi^0 \rightarrow K_L^0 \pi^0 \pi^0$ where both the K_L^0 and π^0 from the K^{*0} are undetected. The Dalitz-plot model of this process is not implemented in our simulation.

making requirements on the energy of showers in the calorimeter that are not associated with the decay products of the $K_S^0 \pi^+ \pi^-$ or the π^0 . We compute the angle, θ , between each unassigned shower and the direction of the missing momentum. For $\cos \theta < 0.9$, we require the energy of showers, $E_{shower} < 100 \text{ MeV}$ for any single shower. If $0.9 < \cos \theta < 0.98$, we require $E_{shower} < 100 + 250 \times (\cos \theta - 0.9) \text{ MeV}$. The M_{miss}^2 distribution for $K_L^0 \pi^0$ is shown in Fig. 5. The points with error bars are data and the shaded histogram represents a simulation of the backgrounds. Signal candidates are required to be within the range $0.1 < M_{miss}^2 < 0.5 \text{ GeV}^2/c^4$.

E. Double tags with $K_L^0 \pi^+ \pi^-$

Candidate $K_L^0 \pi^+ \pi^-$ decays are reconstructed in DTs using a similar missing mass technique as described in Section III D. We require the signal side (associated with the $K_L^0 \pi^+ \pi^-$ candidate) to have exactly two charged tracks. Backgrounds are reduced by applying π^0 , η , and K_S^0 vetoes. Using the measured momenta of the tagged D^0 and the two additional pions, we compute the missing momentum and missing energy on the signal side. We apply

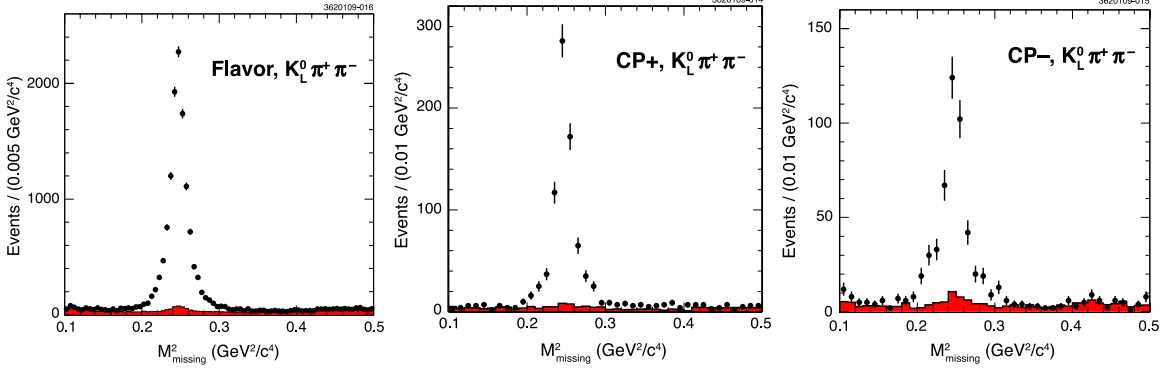


FIG. 6: M_{miss}^2 distributions for $K_L^0 \pi^+ \pi^-$ for flavor tags (left), CP-even tags (middle), and CP-odd tags (right). The points with error bars are data and the shaded histograms represent simulations of the backgrounds.

the same requirements to the energy of the unassigned showers as described in Section III D. The M_{miss}^2 distributions for $K_L^0 \pi^+ \pi^-$ are shown in Fig. 6. The points with uncertainties are data and the shaded histograms show a simulation of the backgrounds. Signal events are required to have a missing-mass squared in the region $0.21 < M_{miss}^2 < 0.29 \text{ GeV}^2/c^4$.

F. Yields in Data

The ST yields for the tag modes and DT yields for $K_{S/L}^0 \pi^+ \pi^-$ versus different tags are shown in Table III. To determine the $D^0 \rightarrow K^- e^+ \nu$ and $D^0 \rightarrow K_L^0 \pi^0$ ST yields we use the integrated luminosity, measured $D^0 \bar{D}^0$ cross-sections [11] and measured branching fractions [18, 19]. Combining all modes of the same CP, we show in Fig. 7 the Dalitz-plot distribution of CP-even and CP-odd tagged $\tilde{D}^0 \rightarrow K_S^0 \pi^+ \pi^-$ decays. Figure 8 shows the corresponding distributions for CP-tagged $\tilde{D}^0 \rightarrow K_L^0 \pi^+ \pi^-$ decays. The clear absence of a $\rho^0 K_S^0$ component (CP-odd) in CP-odd tagged $K_S^0 \pi^+ \pi^-$ decays is an illustration of the quantum correlations that exist in the $\psi(3770) \rightarrow D^0 \bar{D}^0$ decay. For $K_L^0 \pi^+ \pi^-$, $\rho^0 K_L^0$ is absent in the CP-even tagged samples.

The signal-to-background ratios in our $K_{S/L}^0 \pi^+ \pi^-$ DT samples range from 10 to better than 100, depending on tag mode. The tag side ΔE , K_S^0 and ω sidebands are used for combinatorial and non-resonant background subtraction. On the signal side, the background level is 1.9% for $K_S^0 \pi^+ \pi^-$ after applying the K_S^0 flight significance requirement. This part of the background is considered as a systematic error. The background-to-signal ratio for the $K_L^0 \pi^+ \pi^-$ signal side is about 5%, of which about 2% is a peaking background from $K_S^0 \pi^+ \pi^-$, $K_S^0 \rightarrow \pi^0 \pi^0$ decays that pass the $K_L^0 \pi^+ \pi^-$ selection criteria. We estimate this peaking background yield using $K_S^0 \pi^+ \pi^-$ data and a misidentification rate determined from a quantum-correlated Monte Carlo simulation. The combinatorial background contribution is estimated using the M_{miss}^2 sidebands. The expected yields from these two background sources are subtracted from the observed signal yields to obtain background-corrected yields.

For the $K_S^0 \pi^+ \pi^-$ vs. $K_S^0 \pi^+ \pi^-$ sample, no K_S^0 flight significance requirement was applied, resulting in a background-to-signal ratio of $\sim 9\%$. About 7% (of 9%) of this background comes from $\tilde{D}^0 \rightarrow \pi^+ \pi^- \pi^+ \pi^-$ faking $K_S^0 \pi^+ \pi^-$. This background is subtracted using a Monte Carlo simulation of this decay, where the $\pi^+ \pi^- \pi^+ \pi^-$ Dalitz-plot structure is taken

TABLE III: Single tag and $K_{S/L}^0\pi^+\pi^-$ double tag yields.

Mode	ST Yield	$K_S^0\pi^+\pi^-$ yield	$K_L^0\pi^+\pi^-$ yield
Flavor Tags			
$K^-\pi^+$	144563 ± 403	1447	2858
$K^-\pi^+\pi^0$	258938 ± 581	2776	5130
$K^-\pi^+\pi^+\pi^-$	220831 ± 541	2250	4110
$K^-e^+\nu$	123412 ± 4591	1356	-
CP-Even Tags			
K^+K^-	12867 ± 126	124	345
$\pi^+\pi^-$	5950 ± 112	62	172
$K_S^0\pi^0\pi^0$	6562 ± 131	56	-
$K_L^0\pi^0$	27955 ± 2013	229	-
CP-Odd Tags			
$K_S^0\pi^0$	19059 ± 150	189	281
$K_S^0\eta$	2793 ± 69	39	41
$K_S^0\omega$	8512 ± 107	83	-
$K_S^0\pi^+\pi^-$	-	475	867

from the FOCUS experiment [20]. The impact of the remaining $\sim 1.9\%$ of background on our nominal fit results is small and included in the systematic uncertainties.

The reconstruction efficiency is defined as the ratio of reconstructed events to generated events in each bin. The reconstruction efficiencies are calculated from large Monte Carlo samples generated according to the amplitude description of Eqs. 7 and 9 for different tag modes. Dividing the observed yields in each δ_D bin by this efficiency, we obtain the efficiency-corrected yields, M_i^\pm and M_{ij} .

IV. EXTRACTION OF c_i AND s_i

We determine the coefficients c_i , s_i by minimizing the negative log-likelihood function

$$\begin{aligned}
 -2\log\mathcal{L} = & -2\sum_i \log P(M_i^\pm, \langle M_i^\pm \rangle)_{(CP, K_S^0\pi^+\pi^-)} \\
 & -2\sum_i \log P(M_i^\pm, \langle M_i^\pm \rangle)_{(CP, K_L^0\pi^+\pi^-)} \\
 & -2\sum_{i,j} \log P(M_{ij}, \langle M_{ij} \rangle)_{(K_S^0\pi^+\pi^-, K_S^0\pi^+\pi^-)} \\
 & -2\sum_{i,j} \log P(M_{ij}, \langle M_{ij} \rangle)_{(K_S^0\pi^+\pi^-, K_L^0\pi^+\pi^-)} \\
 & +\chi^2,
 \end{aligned} \tag{15}$$

where $\langle M_i^\pm \rangle$ is calculated according Eqs. 8 and 11, and $\langle M_{ij} \rangle$ is calculated according Eqs. 10 and 12, and $P(M, \langle M \rangle)$ is the Poisson probability to get M events given the expected

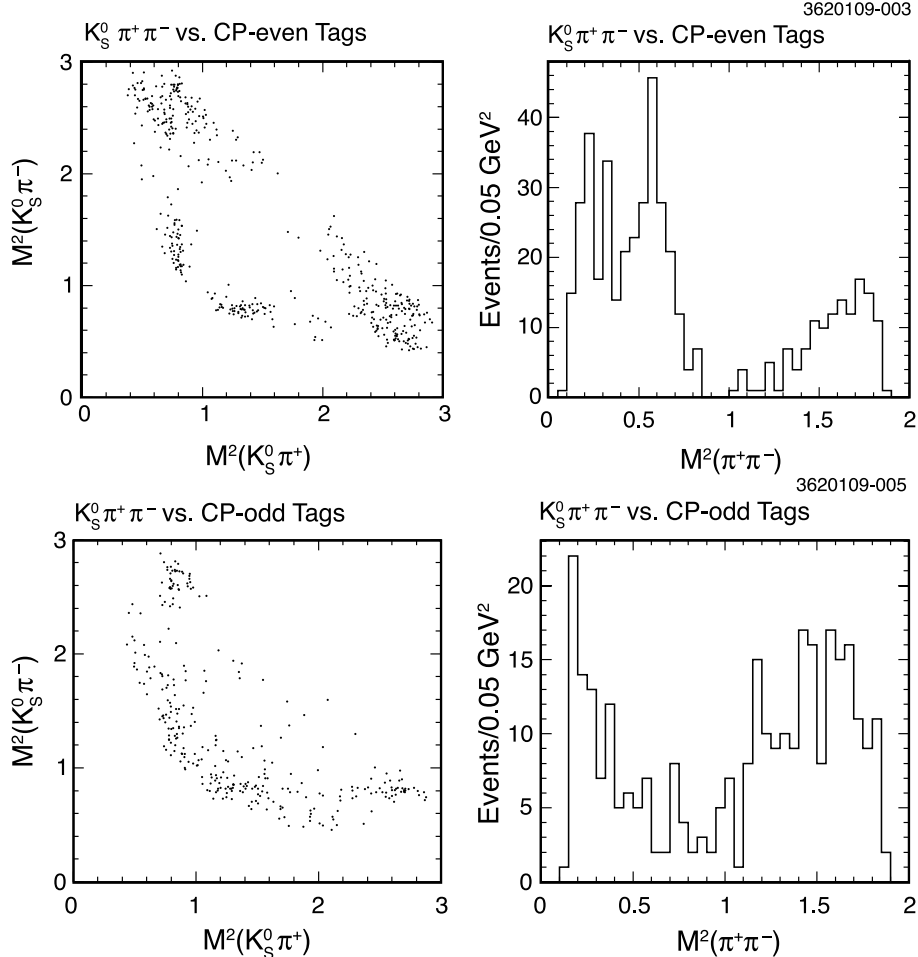


FIG. 7: CP-even tagged $K_S^0 \pi^+ \pi^-$ Dalitz plot (a), and its $m^2(\pi^+ \pi^-)$ projection (b). CP-odd tagged $K_S^0 \pi^+ \pi^-$ Dalitz plot (c), and its $m^2(\pi^+ \pi^-)$ projection (d).

number, $\langle M \rangle$. In our nominal fit, a χ^2 penalty term

$$\chi^2 = \sum_i \left(\frac{c'_i - c_i - \Delta c_i}{\delta \Delta c_i} \right)^2 + \sum_i \left(\frac{s'_i - s_i - \Delta s_i}{\delta \Delta s_i} \right)^2, \quad (16)$$

constrains c'_i and s'_i to differ from c_i and s_i , respectively, by their expected differences Δc_i , Δs_i , within errors. (Those errors, $\delta \Delta c_i$, $\delta \Delta s_i$, are the systematic uncertainties shown in Table I.) This constraint has little impact on c_i but is important for s_i and will be relaxed and tightened as a systematic variation.

From Monte Carlo studies, we found that DCSD decays in flavor tag modes ($K^- \pi^+$, $K^- \pi^+ \pi^0$, $K^- \pi^+ \pi^+ \pi^-$) lead to a significant bias in the $K_i^{(\prime)}$'s due to an interference of the wrong flavor of the $\tilde{D}^0 \rightarrow K_{S/L}^0 \pi^+ \pi^-$ decay; this results in a significant bias in the values of $c_i^{(\prime)}$ and $s_i^{(\prime)}$ from the $D^0 \rightarrow K_S^0 \pi^+ \pi^-$ vs. $D^0 \rightarrow K_{S/L}^0 \pi^+ \pi^-$ analyses. Therefore, for the $D^0 \rightarrow K_L^0 \pi^+ \pi^-$ vs. $D^0 \rightarrow K_S^0 \pi^+ \pi^-$ analysis, we use only the $D^0 \rightarrow K^- e^+ \nu$ tagged $K_S^0 \pi^+ \pi^-$ sample and the $D^0 \rightarrow K^- \pi^+$ tagged $K_L^0 \pi^+ \pi^-$ sample for counting $S_f^{(\prime)}$ and $K_i^{(\prime)}$ yields.² For

² All three hadronic flavor tag modes are used to determine $K_i^{(\prime)}$ for the CP-tag vs. $K_{S/L}^0 \pi^+ \pi^-$ determina-

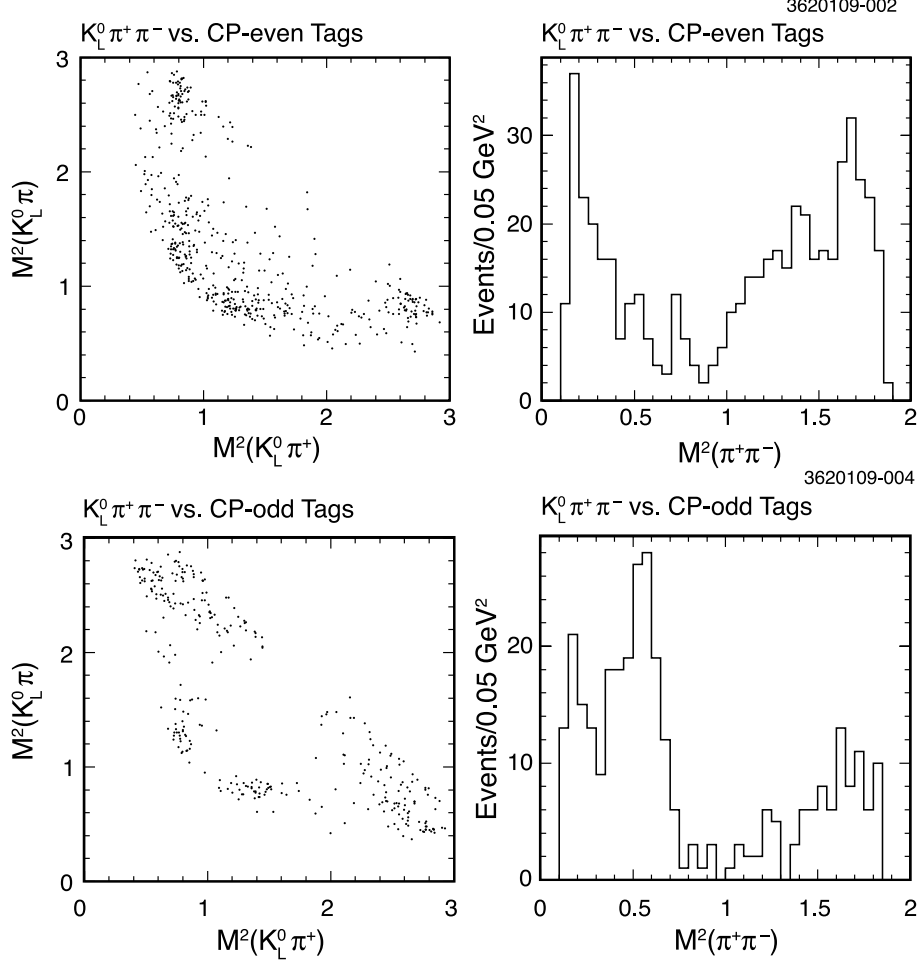


FIG. 8: CP-even tagged $K_L^0 \pi^+ \pi^-$ Dalitz plot (a), and its $m^2(\pi^+ \pi^-)$ projection (b). CP-odd tagged $K_L^0 \pi^+ \pi^-$ Dalitz plot (c), and its $m^2(\pi^+ \pi^-)$ projection (d).

the latter, we estimate the biases and adjust the $K_i^{(\prime)}$ values using the correction factor:

$$|A_{D^0 \rightarrow K_S^0 \pi^+ \pi^-}|^2 / |A_{D^0 \rightarrow K_S^0 \pi^+ \pi^-} + r e^{-i\delta} A_{\bar{D}^0 \rightarrow K_S^0 \pi^+ \pi^-}|^2.$$

Here $r = |A(D^0 \rightarrow K^+ \pi^-) / A(D^0 \rightarrow K^- \pi^+)|$ and $\delta_{K\pi}$ are the ratio of amplitudes of the DCSD to CF decay and the relative strong phase, respectively. The amplitude ratio squared, $r^2 = (3.44 \pm 0.01 \pm 0.09) \times 10^{-3}$ and $\delta_{K\pi} = (22 \pm 16.3)^\circ$ are taken from Ref. [16]. This correction factor is estimated in each of our eight Dalitz-plot bins using the BaBar $D^0 \rightarrow K_S^0 \pi^+ \pi^-$ Dalitz-plot fit amplitude [4]. The model dependence of this correction is negligible. Uncertainties on these corrections due to the uncertainty on $\delta_{K\pi}$ are small and are included in our systematic uncertainties.

The fitting procedure was tested using a simulated C -odd $D^0 \bar{D}^0$ Monte Carlo sample where we performed 100 toy $K_S^0 \pi^+ \pi^-$ vs. $K_S^0 \pi^+ \pi^-$ experiments with c_i and s_i taken from the BaBar model. The means and widths of the pull distributions of the c_i and s_i parameters

tion of $c_i^{(\prime)}$.

TABLE IV: Fit results for c_i , s_i (with Δc_i and Δs_i fixed), c_i , c'_i , s_i and s'_i (with Δc_i and Δs_i constrained). See Table I for Δc_i and Δs_i .

i	$\Delta c_i, \Delta s_i$ fixed		$\Delta c_i, \Delta s_i$ constrained			
	c_i	s_i	c_i	c'_i	s_i	s'_i
0	0.742 ± 0.037	0.004 ± 0.160	0.743 ± 0.041	0.840 ± 0.041	0.014 ± 0.166	-0.021 ± 0.164
1	0.606 ± 0.071	0.014 ± 0.215	0.611 ± 0.072	0.779 ± 0.072	0.014 ± 0.216	-0.069 ± 0.219
2	-0.008 ± 0.063	0.581 ± 0.190	0.059 ± 0.077	0.250 ± 0.078	0.609 ± 0.188	0.587 ± 0.188
3	-0.529 ± 0.101	0.138 ± 0.217	-0.495 ± 0.114	-0.349 ± 0.135	0.151 ± 0.225	0.275 ± 0.232
4	-0.889 ± 0.049	-0.053 ± 0.183	-0.911 ± 0.053	-0.793 ± 0.057	-0.050 ± 0.189	-0.016 ± 0.192
5	-0.742 ± 0.066	-0.317 ± 0.187	-0.736 ± 0.070	-0.546 ± 0.080	-0.340 ± 0.194	-0.388 ± 0.200
6	0.108 ± 0.074	-0.836 ± 0.185	0.157 ± 0.092	0.475 ± 0.094	-0.827 ± 0.190	-0.725 ± 0.196
7	0.403 ± 0.046	-0.410 ± 0.158	0.403 ± 0.046	0.591 ± 0.048	-0.409 ± 0.158	-0.374 ± 0.169

were consistent with zero and one, respectively, indicating no bias and proper estimation of statistical uncertainties.

To enable the separation of the statistical uncertainty on c_i and s_i from the systematic uncertainty on Δc_i and Δs_i we perform a likelihood fit to (c_i, s_i) with the values of (c'_i, s'_i) fixed according to Table I. The results of this fit and of the nominal likelihood fit to (c_i, s_i) , (c'_i, s'_i) are shown in Table IV. The (statistical) correlation matrix among c_i and s_i in the constrained fit is shown in Table V. Note that in Table IV, we choose the s_i and s'_i signs based on BaBar isobar model predictions [4] to resolve the two-fold ambiguity discussed in Section II.

TABLE V: Correlation Matrix for the c_i and s_i parameters. Labels 1-8 represents $c_1 - c_8$ and 9-16 represent $s_1 - s_8$.

i	1	2	3	4	5	6	7	8	9	10	11	12	13	14	15	16
1	1.000															
2	-0.028	1.000														
3	-0.007	-0.011	1.000													
4	0.035	0.011	0.002	1.000												
5	0.073	-0.022	0.006	0.004	1.000											
6	0.016	0.069	-0.003	0.003	-0.104	1.000										
7	0.018	0.013	-0.020	0.005	0.033	0.016	1.000									
8	-0.020	-0.028	0.008	0.005	0.050	0.013	0.015	1.000								
9	0.024	0.006	-0.072	-0.006	0.014	0.014	0.113	0.040	1.000							
10	0.000	-0.033	0.017	-0.007	-0.003	0.038	-0.001	-0.001	-0.060	1.000						
11	0.006	0.007	-0.025	-0.002	0.003	-0.008	0.041	0.029	0.323	-0.154	1.000					
12	0.004	0.005	-0.020	0.035	0.002	0.000	0.014	0.005	0.149	-0.124	0.244	1.000				
13	0.001	-0.001	-0.003	-0.014	-0.008	-0.072	-0.007	-0.004	0.158	-0.107	0.340	0.070	1.000			
14	-0.011	-0.014	0.078	0.005	-0.004	-0.042	-0.086	-0.021	-0.448	0.085	-0.213	-0.124	-0.275	1.000		
15	0.009	0.008	-0.053	-0.003	0.004	0.002	0.061	0.013	0.373	-0.139	0.314	0.228	0.269	-0.405	1.000	
16	0.004	0.004	-0.056	-0.004	0.003	-0.007	0.026	0.041	0.234	-0.096	0.521	0.176	0.243	-0.133	0.106	1.000

V. SYSTEMATIC UNCERTAINTIES

Systematic uncertainties on (c_i, s_i) and (c'_i, s'_i) come from many sources. Table VI and Table VII summarize the main contributions of the systematic uncertainties for c_i and s_i ,

respectively. Table VIII and Table IX summarize the main contributions of the systematic uncertainties for c'_i and s'_i , respectively.

TABLE VI: Systematic uncertainties for c_i .

	c_1	c_2	c_3	c_4	c_5	c_6	c_7	c_8
$K_i^{(\prime)}$ statistics error	0.010	0.015	0.016	0.019	0.009	0.015	0.018	0.008
Momentum resolution	0.008	0.015	0.012	0.019	0.011	0.012	0.017	0.009
Efficiency variation	0.004	0.007	0.011	0.008	0.005	0.008	0.010	0.006
Single Tag yields	0.006	0.007	0.013	0.011	0.005	0.008	0.015	0.008
Tag side background	0.007	0.007	0.014	0.013	0.006	0.008	0.014	0.011
$K_S^0\pi^+\pi^-$ background	0.001	0.002	0.009	0.027	0.012	0.006	0.003	0.002
$K_L^0\pi^+\pi^-$ background	0.006	0.018	0.004	0.024	0.017	0.012	0.020	0.006
Multi-Candidate selection	0.002	0.003	0.003	0.008	0.004	0.006	0.003	0.002
Non- D/\bar{D}	0.010	0.016	0.004	0.007	0.004	0.005	0.006	0.005
DCSD	0.009	0.012	0.005	0.013	0.014	0.010	0.013	0.006
Sum	0.022	0.037	0.031	0.052	0.032	0.030	0.042	0.021

TABLE VII: Systematic uncertainties for s_i .

	s_1	s_2	s_3	s_4	s_5	s_6	s_7	s_8
$K_i^{(\prime)}$ statistics error	0.031	0.027	0.039	0.030	0.023	0.023	0.033	0.026
Momentum resolution	0.018	0.035	0.023	0.033	0.023	0.022	0.022	0.018
Efficiency variation	0.018	0.012	0.019	0.010	0.013	0.018	0.013	0.012
Single Tag yields	0.005	0.001	0.005	0.004	0.003	0.003	0.005	0.003
Tag side background	0.004	0.001	0.001	0.003	0.001	0.004	0.002	0.001
$K_S^0\pi^+\pi^-$ background	0.005	0.008	0.030	0.023	0.005	0.003	0.016	0.014
$K_L^0\pi^+\pi^-$ background	0.050	0.022	0.018	0.035	0.006	0.024	0.005	0.025
Multi-Candidate selection	0.036	0.018	0.033	0.012	0.022	0.026	0.028	0.011
Non- D/\bar{D}	0.005	0.003	0.004	0.005	0.005	0.005	0.003	0.002
DCSD	0.023	0.004	0.030	0.019	0.015	0.006	0.027	0.020
Sum	0.077	0.055	0.076	0.069	0.045	0.052	0.060	0.050

In the global fit, the fitter does not take the statistical uncertainties associated with flavor tagged samples into account. We estimate this part of the uncertainties by varying the input variables ($K_i^{(\prime)}$) one by one according to their statistical uncertainties, and by making new fits. At the end, we take the quadratic sum of all the variations as the systematic error.

Since our Dalitz-plot binning results in bins with unusual shapes and in some cases very narrow regions (see Fig. 1), the migration of events from one bin to another bin may bias our result. The position of an event in the Dalitz plot depends on its momentum determination. The systematic error associated with momentum resolution is studied by smearing the momentum of a fully simulated Monte Carlo 200 times, according to the CLEO detector momentum resolution. The distributions of the results for (c_i, s_i) and (c'_i, s'_i) are then fitted with Gaussian functions, and the widths of the distributions are taken as the systematic uncertainties.

The systematic uncertainties associated with $K_{S/L}^0\pi^+\pi^-$ finding cancel under the assumption that the efficiency systematic uncertainties are uniform across the Dalitz plot. Under

TABLE VIII: Systematic uncertainties for c'_i .

	c_1	c_2	c_3	c_4	c_5	c_6	c_7	c_8
$K_i^{(\prime)}$ statistics error	0.009	0.014	0.011	0.013	0.009	0.012	0.017	0.008
Momentum resolution	0.008	0.016	0.014	0.020	0.010	0.013	0.019	0.010
Efficiency variation	0.006	0.006	0.009	0.009	0.004	0.007	0.011	0.006
Single Tag yields	0.005	0.007	0.007	0.007	0.003	0.005	0.006	0.007
Tag side background	0.005	0.007	0.007	0.007	0.004	0.005	0.005	0.009
$K_S^0\pi^+\pi^-$ background	0.002	0.001	0.005	0.012	0.007	0.003	0.001	0.002
$K_L^0\pi^+\pi^-$ background	0.008	0.020	0.017	0.046	0.019	0.014	0.015	0.006
Multi-Candidate selection	0.003	0.003	0.001	0.004	0.003	0.004	0.002	0.002
Non- D/\bar{D}	0.012	0.018	0.005	0.006	0.004	0.004	0.008	0.005
DCSD	0.011	0.013	0.007	0.013	0.014	0.013	0.014	0.006
Sum	0.023	0.039	0.029	0.057	0.029	0.028	0.036	0.021

 TABLE IX: Systematic uncertainties for s'_i .

	c_1	c_2	c_3	c_4	c_5	c_6	c_7	c_8
$K_i^{(\prime)}$ statistics error	0.030	0.028	0.037	0.026	0.022	0.025	0.034	0.028
Momentum resolution	0.022	0.042	0.031	0.042	0.029	0.028	0.031	0.033
Efficiency variation	0.018	0.012	0.015	0.009	0.012	0.018	0.013	0.013
Single Tag yields	0.005	0.001	0.005	0.003	0.004	0.003	0.004	0.003
Tag side background	0.003	0.000	0.002	0.002	0.002	0.004	0.003	0.001
$K_S^0\pi^+\pi^-$ background	0.006	0.009	0.028	0.021	0.004	0.003	0.015	0.015
$K_L^0\pi^+\pi^-$ background	0.052	0.022	0.013	0.033	0.003	0.025	0.004	0.025
Multi-Candidate selection	0.038	0.018	0.031	0.007	0.020	0.027	0.028	0.013
$\delta\Delta c_i, \delta\Delta s_i$	0.034	0.048	0.001	0.006	0.009	0.072	0.050	0.048
Non- D/\bar{D}	0.005	0.003	0.004	0.005	0.004	0.005	0.003	0.002
DCSD	0.021	0.005	0.028	0.016	0.013	0.007	0.028	0.022
Sum	0.080	0.060	0.072	0.067	0.046	0.056	0.065	0.059

this condition Eq. 8, Eq. 10, Eq. 11, and Eq. 12 have the same dependence on efficiency. To account for a small non-uniformity, we generate a large number of toy experiments where we randomly distribute the efficiency of each bin according to a Gaussian distribution (width is taken as 0.02) and repeat this process for many times. The widths of the resulting distributions for (c_i, s_i) and (c'_i, s'_i) are taken as systematic uncertainties.

The systematic uncertainties associated with the single tag yields are evaluated by repeating the fit with the input values varied by their own uncertainties. Assuming the contributions are uncorrelated, we sum in quadrature to obtain the uncertainties on (c_i, s_i) and (c'_i, s'_i) due to single tag yields given in Table VI - Table IX.

The systematic uncertainties due to the estimation of the tag side background are studied mode by mode, and the quadratic sum is given in Table VI - Table IX.

Though we used ΔE and $M(\pi^+\pi^-)$ mass sidebands for the tag side backgrounds subtraction, we did not apply any background subtraction for $K_S^0\pi^+\pi^-$ signal side, which is believed to be small since we require the decay vertex of K_S^0 to be separated from the interaction region with a significance greater than two standard deviations. The background

level in the signal region is estimated from $M(\pi^+\pi^-)$ sidebands. We found there is about a 1.9% background in the signal region. The systematic uncertainties due to this part of the background are estimated using Quantum Correlated Monte Carlo samples. We estimate the background contributions from Quantum Correlated Monte Carlo samples, then make a new fit with the background subtracted. The differences of the results between the nominal fit and the new fit are taken as the systematic uncertainties.

The systematic uncertainties due to the $K_L^0\pi^+\pi^-$ background shape are considered by repeating the fit assuming the background across the Dalitz plot is uniform. The uncertainties due to the estimation of the background level are negligible. The systematic uncertainties due to flavor-tagged, CP-even tagged, CP-odd tagged, and $K_S^0\pi^+\pi^-$ tagged $K_L^0\pi^+\pi^-$ samples are considered separately and summed in quadrature in Table VI - Table IX.

It is possible to select a wrong combination when there are multiple signal candidates in an event, especially for $K_S^0\pi^+\pi^-$ vs. $K_{S/L}^0\pi^+\pi^-$ samples, since there are many pions with similar momenta. The systematic uncertainties are studied by applying correction matrices to the yield matrices M_{ij} . The corrections are typically 2% (5%) for the $K_S^0\pi^+\pi^-$ vs. $K_S^0\pi^+\pi^-$ ($K_S^0\pi^+\pi^-$ vs. $K_L^0\pi^+\pi^-$) event samples.

Monte Carlo simulated continuum events are checked for non- D^0/\bar{D}^0 backgrounds. No significant peaking background is seen for double tagged $K_S^0\pi^+\pi^-$ samples. The contributions for K^+K^- , $\pi^+\pi^-$, and $K_S^0\eta$ tagged $K_L^0\pi^+\pi^-$ samples are also negligible. For other samples, there are 1~2% contributions depending on the tag mode. A systematic study is performed by assuming the background is uniformly distributed over the Dalitz plot.

For the DCSD effect, we made corrections to $K^-\pi^+$ vs. $K_{S,L}^0\pi^+\pi^-$ yields in Section IV by using results from Ref. [16]. The systematic uncertainties due to r is negligible since it is precisely measured. The systematic uncertainties due to the strong phase δ are studied by varying it according to its error. For $K^-\pi^+\pi^0$, and $K^-\pi^+\pi^+\pi^-$ tag modes, there are no relative strong phase measurements, so we consider four cases, $\delta = (0^\circ, 90^\circ, 180^\circ, 270^\circ)$, and take the maximum variations among the four cases as the systematic uncertainty.

The total systematic uncertainties on (c_i, s_i) and (c'_i, s'_i) – excluding the systematic uncertainty on Δc_i and Δs_i that relate the $K_S^0\pi^+\pi^-$ and $K_L^0\pi^+\pi^-$ Dalitz-plot models – are obtained from the quadrature sum of these systematic uncertainties, are shown in Tables VI - Table IX.

In the global fit, Δc_i and Δs_i are constrained using a χ^2 term. The errors on Δc_i and Δs_i are determined by comparing BaBar, Belle, and CLEO II $D^0 \rightarrow K_S^0\pi^+\pi^-$ Dalitz-plot fit results. The constraint on c and c' can be removed with little impact on the result. The constraint on s and s' can be relaxed to a factor of 4, but cannot be removed entirely, otherwise, the fit does not converge. To assess our sensitivity to this constraint we consider the following 1) we relax the constraint by a factor of 2, *i.e.* increase the errors by a factor of 2 and re-fit the data. 2) we fix Δc_i and Δs_i and re-fit the data (see Table IV). The maximum difference for each (c_i, s_i) and (c'_i, s'_i) between these fits and the nominal fit is interpreted as the systematic uncertainty. An alternate assessment of this systematic uncertainty is the difference in quadrature of the errors reported for the “fixed” and “constrained” fits reported in Table IV. The quadrature average of these two methods is reported as the third error on (c_i, s_i) and (c'_i, s'_i) in Table X and Table XI, respectively.

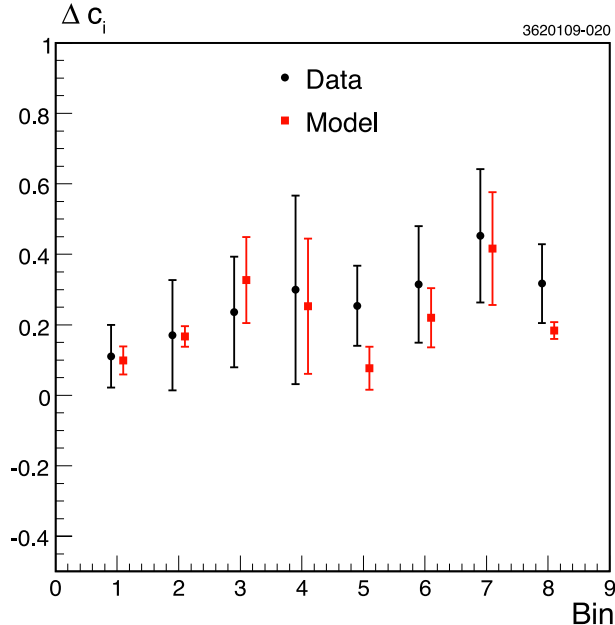


FIG. 9: Comparison of $\Delta c_i = c'_i - c_i$ between CP-tagged $K_{S/L}^0 \pi^+ \pi^-$ CLEO-c data (circles) and predictions from the BaBar model (squares).

VI. CROSS CHECK FOR MODEL PREDICTIONS

Using CP-tagged $K_{S/L}^0 \pi^+ \pi^-$ samples, we can get c_i and c'_i without any correlations, so the differences between c_i and c'_i provide a good test of our predictions on the differences discussed in Section II. The comparison between measured $\Delta c_i = c'_i - c_i$ and the BaBar model predictions is shown in Fig. 9. We find good agreement between the data and the results obtained using the BaBar model, modified to account for the difference between $D^0 \rightarrow K_S^0 \pi^+ \pi^-$ and $D^0 \rightarrow K_L^0 \pi^+ \pi^-$.

VII. FINAL RESULTS AND IMPACT ON γ/ϕ_3 MEASUREMENT

Our final results for c_i , s_i , c'_i and s'_i are shown in Table X and Table XI, respectively. The statistical uncertainties dominate for c_i and s_i . The systematic uncertainty due to Δc_i and Δs_i which relate the strong phase difference of $D^0 \rightarrow K_S^0 \pi^+ \pi^-$ and $D^0 \rightarrow K_L^0 \pi^+ \pi^-$ is comparable to – but does not dominate – all other contributions to the total systematic uncertainty.

To see the impact of our results on the γ/ϕ_3 measurement, we generate toy Monte Carlo $B^\pm \rightarrow \tilde{D}^0 K^\pm$ samples with $\gamma/\phi_3 = 60^\circ$, $\delta_B = 130^\circ$ and $r_B = 0.1$. The $B^\pm \rightarrow \tilde{D}^0 K^\pm$ sample is large enough so that the statistical uncertainty associated with B decays is negligible. We assume the reconstruction efficiency is 100% and that no background is present. We fit for γ/ϕ_3 , δ_B , and r_B 10,000 times by sampling c_i and s_i according to their uncertainties and correlations. We find the width of the resulting γ/ϕ_3 distribution, shown in Fig. 10, is about 1.7° . However, a small bias of 0.5° is observed, which is believed to be caused by the unphysical c_i and s_i pairs (617 out of 8000) with $c_i^2 + s_i^2 > 1$.

Comparing with a model uncertainty of 7° for BaBar [5] and 9° for Belle [6], great

TABLE X: Fit results for c_i and s_i . The first error is statistical, the second error is the systematic uncertainty (excluding $\Delta c_i, \Delta s_i$), the third error is the systematic uncertainty due to Δc_i and Δs_i that relate the $K_S^0\pi^+\pi^-$ and $K_L^0\pi^+\pi^-$ Dalitz-plot models .

i	c_i	s_i
0	$0.743 \pm 0.037 \pm 0.022 \pm 0.013$	$0.014 \pm 0.160 \pm 0.077 \pm 0.045$
1	$0.611 \pm 0.071 \pm 0.037 \pm 0.009$	$0.014 \pm 0.215 \pm 0.055 \pm 0.017$
2	$0.059 \pm 0.063 \pm 0.031 \pm 0.057$	$0.609 \pm 0.190 \pm 0.076 \pm 0.037$
3	$-0.495 \pm 0.101 \pm 0.052 \pm 0.045$	$0.151 \pm 0.217 \pm 0.069 \pm 0.048$
4	$-0.911 \pm 0.049 \pm 0.032 \pm 0.021$	$-0.050 \pm 0.183 \pm 0.045 \pm 0.036$
5	$-0.736 \pm 0.066 \pm 0.030 \pm 0.018$	$-0.340 \pm 0.187 \pm 0.052 \pm 0.047$
6	$0.157 \pm 0.074 \pm 0.042 \pm 0.051$	$-0.827 \pm 0.185 \pm 0.060 \pm 0.036$
7	$0.403 \pm 0.046 \pm 0.021 \pm 0.002$	$-0.409 \pm 0.158 \pm 0.050 \pm 0.002$

TABLE XI: Fit results for c'_i and s'_i . The first error is statistical, the second error is the systematic uncertainty (excluding $\Delta c_i, \Delta s_i$), the third error is the systematic uncertainty due to Δc_i and Δs_i

i	c'_i	s'_i
0	$0.840 \pm 0.037 \pm 0.023 \pm 0.014$	$-0.021 \pm 0.160 \pm 0.080 \pm 0.036$
1	$0.779 \pm 0.071 \pm 0.039 \pm 0.008$	$-0.069 \pm 0.215 \pm 0.060 \pm 0.047$
2	$0.250 \pm 0.063 \pm 0.029 \pm 0.102$	$0.587 \pm 0.190 \pm 0.072 \pm 0.006$
3	$-0.349 \pm 0.101 \pm 0.057 \pm 0.092$	$0.275 \pm 0.217 \pm 0.067 \pm 0.058$
4	$-0.793 \pm 0.049 \pm 0.029 \pm 0.036$	$-0.016 \pm 0.183 \pm 0.046 \pm 0.042$
5	$-0.546 \pm 0.066 \pm 0.028 \pm 0.038$	$-0.388 \pm 0.187 \pm 0.056 \pm 0.072$
6	$0.475 \pm 0.074 \pm 0.026 \pm 0.081$	$-0.725 \pm 0.185 \pm 0.065 \pm 0.058$
7	$0.591 \pm 0.046 \pm 0.021 \pm 0.011$	$-0.374 \pm 0.158 \pm 0.059 \pm 0.054$

improvement on the γ/ϕ_3 measurement can be achieved by using a model-independent approach incorporating CLEO-c's results on the strong phase parameters c_i and s_i presented in this article. This will be realized at LHCb where using 10 fb^{-1} of data a *statistical* error on γ/ϕ_3 of 5.5° is anticipated [7]. The weight of $B \rightarrow \tilde{D}K, \tilde{D} \rightarrow K_S^0\pi^+\pi^-$ in the combination of tree-level γ measurements at LHCb, which is predicted to have sensitivity of $1^\circ - 2^\circ$ [21], depends upon the CLEO-c's results on the strong phase parameters c_i and s_i presented in this article.

Sensitivity to New Physics is obtained through the comparison of γ/ϕ_3 measured directly in tree-level processes and indirect determinations of γ/ϕ_3 . One indirect determination, $\gamma/\phi_3 = (67_{-4}^{+5})^\circ$, arises from the intersection of the $B_{(s)}$ mixing and $\sin 2\beta$ contours in the $(\bar{\rho}, \bar{\eta})$ plane [22]. The uncertainty is dominated by the LQCD calculations for mixing [23] and are expected to improve. Another determination of γ/ϕ_3 follows from the unitarity constraint $\gamma = 180^\circ - \alpha - \beta = (70_{-5}^{+6})^\circ$. Here the uncertainty is dominated by the determination of $\alpha/\phi_1 = (88_{-5}^{+6})^\circ$ from $B \rightarrow \pi\pi, \rho\pi, \rho\rho$ [22].

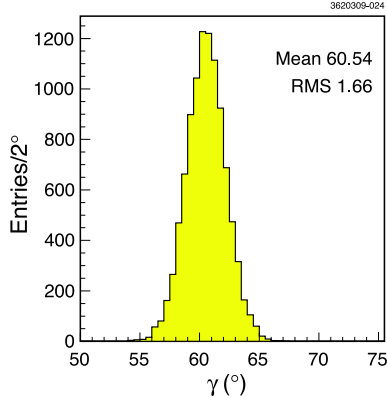


FIG. 10: Toy Monte Carlo Fit Results for γ/ϕ_3 .

VIII. SUMMARY

In summary, using 818 pb^{-1} of e^+e^- collisions produced at the $\psi(3770)$, we make a first determination of the strong phase parameters, c_i and s_i , in Table X. From a toy Monte Carlo study with a large sample of $B^\pm \rightarrow \tilde{D}^0 K^\pm$ data generated with $\gamma/\phi_3 = 60^\circ$, $\delta_B = 130^\circ$ and $r_B = 0.1$, we find that the decay model uncertainty on γ/ϕ_3 is reduced to about 1.7° due to these new measurements. As a result, the precision of the γ/ϕ_3 measurement using $B^+ \rightarrow \tilde{D}^0 K^+$ decays will not be limited by the strong interference effects in the $\tilde{D}^0 \rightarrow K_S^0 \pi^+ \pi^-$ decay. The improved precision in the direct determination of γ/ϕ_3 enabled by this measurement of the strong phase parameters c_i and s_i enhances sensitivity to New Physics through the comparison with indirect determinations of γ/ϕ_3 .

IX. ACKNOWLEDGMENTS

We gratefully acknowledge the effort of the CESR staff in providing us with excellent luminosity and running conditions. D. Cronin-Hennessy and A. Ryd thank the A.P. Sloan Foundation. This work was supported by the National Science Foundation, the U.S. Department of Energy, the Natural Sciences and Engineering Research Council of Canada, and the U.K. Science and Technology Facilities Council.

-
- [1] N. Cabibbo, Phys. Rev. Lett. **10**, 531 (1963); M. Kobayashi and T. Maskwaa, Prog. Theor. Phys. **49**, 652 (1973).
 - [2] A. Giri, Y. Grossman, A. Soffer, and J. Zupan, Phys. Rev. D **68**, 054018 (2003).
 - [3] Y. Grossman, A. Soffer and J. Zupan, Phys. Rev. D **72**, 031501(R) (2005).
 - [4] B. Aubert *et al.* (BaBar Collaboration), Phys. Rev. Lett. **95**, 121802 (2005).
 - [5] B. Aubert *et al.* (BaBar Collaboration), Phys. Rev. D **78**, 034023 (2008).
 - [6] A. Poluektov *et al.* (Belle Collaboration), Phys. Rev. D **70**, 072003 (2004); A. Poluektov *et al.* (Belle Collaboration), Phys. Rev. D **73**, 112009 (2006); K. Abe *et al.* (Belle Collaboration), arXiv:0803.3375 [hep-ex].
 - [7] J. Libby, CERN-LHCB-2007-141, <http://cdsweb.cern.ch/record/1069971?ln=en>.

- [8] A. Bondar *et al.*, Eur. Phys. J. C **47**, 347-353 (2006); A. Bondar and A. Poluektov, Eur. Phys. J. C **55**, 51 (2008).
- [9] H. Muramatsu *et al.* (CLEO Collaboration), Phys. Rev. Lett. **89**, 251802 (2002).
- [10] Y. Kubota *et al.* (CLEO Collaboration), Nucl. Instrum. Methods Phys. Res., Sect. A **320**, 66 (1992); D. Peterson *et al.*, Nucl. Instrum. Methods Phys. Res., Sect. A **478**, 142 (2002); M. Artuso *et al.*, Nucl. Instrum. Methods Phys. Res., Sect. A **554**, 147 (2005).
- [11] S. Dobbs *et al.* (CLEO Collaboration), Phys. Rev. D **76**, 112001 (2007).
- [12] T. E. Coan *et al.* (CLEO Collaboration), Phys. Rev. Lett. **95**, 181802 (2005).
- [13] C. Amsler *et al.*, (Particle Data Group), Phys. Lett. B **667**, 1 (2008).
- [14] S. Kopp *et al.* (CLEO Collaboration), Phys. Rev. D **63**, 092001 (2001).
- [15] J. Adler *et al.* (Mark III Collaboration), Phys. Rev. Lett. **62**, 1821 (1989).
- [16] J. L. Rosner *et al.* (CLEO Collaboration), Phys. Rev. Lett. **100**, 221801 (2008); D. Asner *et al.* (CLEO Collaboration), Phys. Rev. D **78**, 012001 (2008).
- [17] H. Albrecht *et al.* (ARGUS Collaboration), Phys. Lett. B **241**, 278 (1990).
- [18] “Improved Measurements in $D^0 \rightarrow \pi^- e^+ \nu$, $D^0 \rightarrow K^- e^+ \nu$, $D^+ \rightarrow \pi^0 e^+ \nu$, and $D^+ \rightarrow \bar{K}^0 e^+ \nu$ ”, (CLEO Collaboration), to be submitted to Phys. Rev. D - manuscript in preparation.
- [19] Q. He *et al.* (CLEO Collaboration), Phys. Rev. Lett. **100**, 091801 (2008).
- [20] J. M. Link *et al.* (Focus Collaboration), Phys. Rev. D **75**, 052003 (2007).
- [21] K. Akiba *et al.*, CERN-LHCb-2008-031, <http://cdsweb.cern.ch/record/1117819?ln=en>.
- [22] A. Höcker *et al.* (CKMfitter Group), Eur. Phys. J. C **21**, 225 (2001); J. Charles *et al.* (CKMfitter Group), Eur. Phys. J. C **41**, 1 (2005); and updates at <http://ckmfitter.in2p3.fr/>.
- [23] M. Wingate *et al.* (HPQCD Collaboration), Phys. Rev. Lett. **92**, 162001 (2004); A. Gray *et al.* (HPQCD Collaboration), Phys. Rev. Lett. **95**, 212001 (2005); C. Bernard *et al.* (Fermilab Lattice and MILC Collaborations), PoS LAT2007, 370 (2007). S. Aoki *et al.* (JLQCD Collaboration), Phys. Rev. Lett. **91**, 212001 (2003); V. Gadiyak and O. Loktik, Phys. Rev. D **72**, 114504 (2005); N. Tantalo, hep-ph/0703241.